Thermo-mechanical response of metallic sandwich tubes with prismatic cores considering active cooling

Kai Zhang[1], Zichen Deng[*1,2], Huajiang Ouyang[3], Jiaxi Zhou[4], Bo Wang[1]

1 School of Mechanics; Civil Engineering and Architecture, Northwestern Polytechnical University, Xi'an 710072, China

2 State Key Laboratory of Structural Analysis for Industrial Equipment, Dalian University of Technology, Dalian 116024, China

3 School of Engineering, University of Liverpool, Liverpool L69 3GH, United Kingdom

4 College of Mechanical and Vehicle Engineering, Hunan University, Changsha 410082, China

Abstract

In this paper, the transient temperature distribution of sandwich tubes with prismatic cores and the thermo-mechanical responses of the sandwich tubes are analyzed considering active cooling. The effective thermal conductivities of prismatic cores with active cooling are derived. By using the effective thermal conductivities, the transient temperature fields of the tubes are predicted and very close to the results of finite element simulations which reveals the correctness of the effective thermal conductivity. Based on the high order sandwich shell model, the thermal responses of sandwich structures are studied. The thermal responses are also well predicted by the high order displacement theory compared with the results of finite element simulations. The reduction of the thermal responses as a result of active cooling is studied to demonstrate the advantages of prismatic cellular materials. The design of replacing the homo-metal with cellular materials which has the capability of active cooling can reduce the temperature and the thermal structural response of the structure.

Key words: Sandwich tube; Effective thermal conductivity; Active cooling; Transient temperature; Thermal response

1 Introduction

Hollow cylinder is an important kind of structures and widely used in engineering. Especially, when it is used as an engine combustor potentially for aerospace applications[1], there can be massive internal pressures and high working temperature on the structure. The high working temperature and its high-frequency changing will produce very high thermal response which may cause damage and fatigue of the structure. A large body of fundamental researches on the temperature and thermal response of the hollow structure has been carried out over the years [2-5]. However, the method of reducing the temperature have not researched a lot.

* Corresponding author. Professor, E-mail: dweifan@nwpu.edu.cn

Cellular metals have several advantages over monolithic solids, such as light weight, high specific strength, active heat dissipation potential, and other attractive multi-functional characteristics [6-11]. One of interesting applications of cellular metals is active heat dissipation. The structure with an open cell topology especially the lattices (2D) cellular materials has the capability of active heat dissipation to be used as an active cooling panel [12, 13]. Because of the high working temperature and the large temperature gradient on the hollow cylindrical structure used as a combustor engine, the structural design of the tube is very important. The method to design stiff, actively cooled prismatic cellular materials for the combustor liners of next-generation gas turbine engines was studied in [14]. A material selection methodology applicable to lightweight actively cooled panels and their thermo structural performances were studied, particularly suitable for the most demanding aerospace applications [15]. Moreover, the optimal design of the cylindrical structure with thermal boundary conditions was carried out, when the cooling fluid is forced through the cylinder to remove the heat from the inner cell walls [16]. A multi-objective design of lightweight thermo-elastic structure composed of homogeneous porous materials was studied in [17].

As cellular metals exhibit active cooling capability and other favorable properties for multifunctional applications, it is hopeful to replace the hollow solid tube with a prismatic core of cellular metals (Fig. 1) to reduce the temperature by heat exchange between the solid and the fluid forced through the open cell. Hence, the thermal response caused by the high temperature can be reduced, which is good for the structure's life and stability. While it is necessary to get the temperature field of the whole structure before computing the thermal response. Moreover, the thermal conductivity of the structure is a key parameter in calculating the temperature. Meanwhile, the status of the thermal responses of the sandwich tubes with prismatic cores, especially in active cooling process, are still unclear. In this paper, to demonstrate and take the advantage of the multifunctional properties of cellular metals, the thermal conductivity and the temperature field of the hollow tubes with prismatic cores are studied and status of stress are also investigated. The hollow tube is supposed to be replaced by the prismatic cellular metals and it can be treated to be a sandwich structure as a result. The core is divided by a number of revolving periodic unit cells. By deriving the governing equation, the effective thermal conductivity considering active heat dissipation, and the transient temperature field of the structure are obtained. Based on the homogenization method [18] and the {2,1} displacement theory [19, 20], the thermal structural response is determined. The transient temperature and the thermal structural response are compared with the results obtained by the commercial finite element software and are found to be in good agreement. In the end, the effects of active heat dissipation are analyzed.

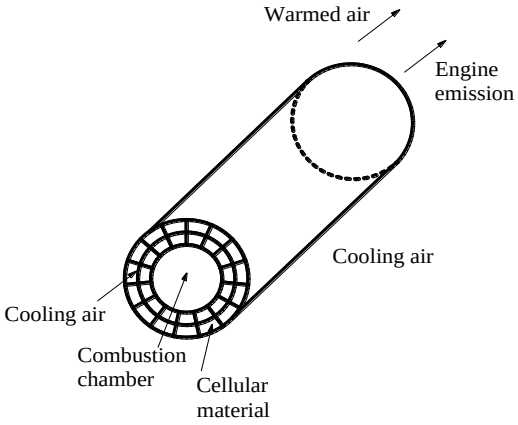

Fig. 1 Schematic diagram

2 Computation model and the effective thermal conductivity

As shown in Fig. 2, the calculation model is a metallic sandwich hollow tube with prismatic cores. It is composed of inner (or bottom) sheet, outer (or top) sheet and the core. Meanwhile the prismatic cores have two topologies which are Square (Fig. 2(b)) and Kagome (Fig. 2(c)) in this paper. It is assumed that the cross-section of the core is divided by 32 revolving periodic unit cells and its reliability have been studied in our pervious paper [21]. A typical cross section and its dimension are shown in Fig. 2(d). The unit cells in Square and Kagome configurations are composed of straight lines or flat plate elements connecting the nodes or nodal lines. a and b are the inner and outer radii of the cylinder, and r_1 and r_2 are the inner and outer radii of the core.

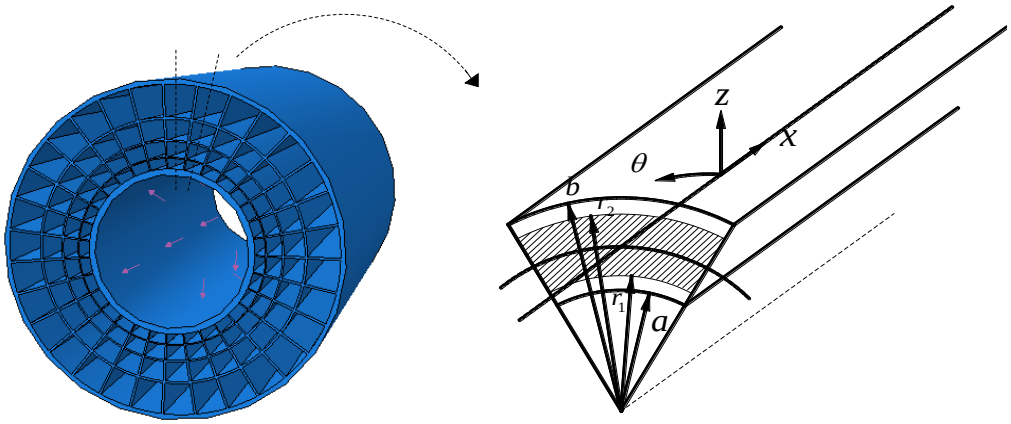

(a) Calculating model

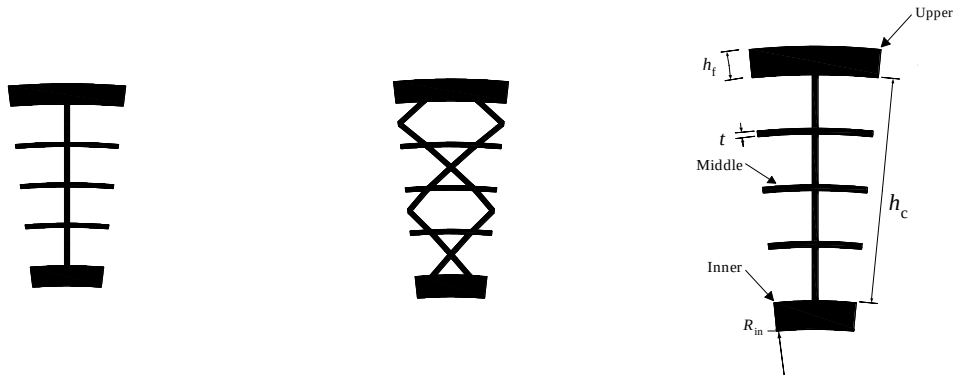

(b) (c) (d)

Fig. 2 **Calculation model**

(a) Calculating model (b) Sandwich cross-section with the Square core (c) Sandwich cross-section with the Kagome core (d) the dimension of the unit cell

As cellular metals have a series of unit cells, the effective thermal conductivity is not easy to obtain and one way of determining it is through homogenizing the prismatic core [20]. However, the effective thermal conductivity only covers the effects of the structural dimension and the physical properties of the metals, but excludes those of the heat transferring among cellular metals and the fluid media. In the process of active heat dissipation, the temperature field not only depends on the heat conductivity of the structure, but also is related to the fluid media running through the open hole (Fig. 2(a)). In this section, the effective thermal conductivity covering the heat dissipation effects is derived for calculating the transient temperature that is then used for obtaining the thermal structural response. Based on studies of Lu and Chen [22], Gu et al. [23] and Zhou et al.[20], the effective heat conductivity without considering the heat transferring between the solids and cool fluid is $\lambda_{\mathrm{r}} = c_{\mathrm{r}}\bar{\rho}\lambda_{\mathrm{s}}$, where

$$\bar{\rho} = \frac{c_1\pi\left(3r_1 + 3/2\,h_{\mathrm{c}}\right)t_{\mathrm{c}} + 4n\left(l_1 + l_2\right)t_{\mathrm{c}} - c_2 n t_{\mathrm{c}}^2}{\pi\left(r_2^2 - r_1^2\right)} \tag{1}$$

$c_r = \dfrac{\xi n t_{\mathrm{c}}}{2\pi\bar{\rho}h_{\mathrm{c}}}$ and $\xi = \ln\left(r_2/r_1\right)$ for the Square, and $c_r = \dfrac{\xi n t_{\mathrm{c}}}{2\pi\bar{\rho}h_{\mathrm{c}}}\dfrac{h_{\mathrm{c}}}{\left(l_1 + l_2\right)}$ and $\xi = \ln\left(r_2/r_1\right)$ for the Kagome. λ_{s} is the heat conductivity of the cellular metals and $\bar{\rho}$ is the relative density. The parameters are listed in Table 1.

Table 1 The parameters of the unit cells

Cell type	c_1	c_2	c_3	l_1	l_2
Square	2	3	12	$\frac{1}{8}h_{\mathrm{c}}$	$\frac{1}{8}h_{\mathrm{c}}$

Kagome	2	10	30	$\left[\left(h_c/4\right)^2+\left(\pi/n\right)^2\left(r_1+h_c/4\right)^2\right]^{1/2}$

It should be noticed that the effective thermal conductivity derived above do not contain the factors of active cooling of the cellular metals. In the next two sections, a new way to obtain the effective thermal conductivity with the factors of active cooling are derived through two steps.

2.1 Steady temperature field of the hollow sandwich tube

The effective heat conductivity obtained above contains the factors of dimensions of the structure and thermal parameters, while the effective heat conductivity considering the active heat dissipation will be derived though the analysis of the steady temperature distribution in the following sections. In the present study, the temperature of the fluid at location *x* is assumed to be only a function of *x*, and the thermal conductivity of the structure is independent of the changing temperature. Based on the effective medium model [23, 24], the governing equation of the temperature field is

$$\left(\frac{\partial^2 T_i(r,x)}{\partial r^2}+\frac{1}{r}\frac{\partial T_i(r,x)}{dr}\right)-\frac{\alpha_{\mathrm{A}} h_i}{\lambda_i}\left(T_i(r,x)-T_{\mathrm{f}}(x)\right)=0 \tag{2}$$

where T_i is the temperature of the i^{th} layer of the sandwich structure, and T_{f} is the temperature of the fluid along the axis of cylinder. α_{A} is the surface area per unit volume and

$$\alpha_{\mathrm{A}}=\frac{2c_1\pi\left(3r_1+3/2\,h_{\mathrm{c}}\right)+8n\left(l_1+l_2\right)-c_3 n t_{\mathrm{c}}}{\pi\left(r_2^2-r_1^2\right)} \tag{3}$$

where λ_i ($i=2$) is the effective thermal conductivity without considering heat dissipation and $\lambda_i=\lambda_{\mathrm{s}}$ ($i=2$). $h=\dfrac{Nu\,k_{\mathrm{f}}}{D_h}$ is the local heat transfer coefficient where Nu is the Nusselt number, k_{f} is the thermal conductivity of the air and $D_{\mathrm{h}}=4\dfrac{1-\bar{\rho}}{\alpha_A}$ is the hydraulic diameter. The solutions of Eq. (2) are obtained as

$$\left.\begin{array}{ll} T_i(r,x)=A_i+B_i\ln\left(r\right) & i=1,3 \\ T_i(r,x)=T_{\mathrm{f}}+A_i I_0\left(m_{\mathrm{c}}r\right)+B_i K_0\left(m_{\mathrm{c}}r\right) & i=2 \end{array}\right\} \tag{4}$$

where I_0 and K_0 are the first and the second kind zero-order modified Bessel functions. The convection boundaries on the inner and outer walls of the hollow

sandwich tube between the surrounding mediums with heat transfer coefficients h_a and h_b are defined in Eq. (5):

$$\begin{cases} \dfrac{\partial T_1}{\partial r} - h_a T_1 = -h_a T_a & r = a \\ T_1 = T_2, \lambda_1 \dfrac{\partial T_1}{\partial r} = \lambda_2 \dfrac{\partial T_2}{\partial r} & r = r_1 \\ T_2 = T_3, \lambda_2 \dfrac{\partial T_2}{\partial r} = \lambda_3 \dfrac{\partial T_3}{\partial r} & r = r_2 \\ \dfrac{\partial T_3}{\partial r} + h_b T_3 = h_b T_b & r = b \end{cases} \tag{5}$$

where T_a and T_b are the temperature of the surrounding mediums of the inner and outer walls. Assuming the heat flowing into the low temperature media is equal to the heat loss through a cross section in a control volume, this process can be described by the equation below

$$\dot{m} c_p \left[T_f \left(x + \mathrm{d}x \right) - T_f \right] = q_1 + q_2 + q_w \tag{6}$$

where $\dot{m} = \rho_f v_0 \pi \left(r_2^2 - r_1^2 \right) \left(1 - \overline{\rho} \right)$, c_p is the specific heat of the air, $q_1 = -\lambda_1 \dfrac{2\pi r_1}{n} \dfrac{dT}{dr}\bigg|_{r=r_1}$ is the heat flux from the inner sheet to the core, $q_2 = -\lambda_3 \dfrac{2\pi r_2}{n} \dfrac{dT}{dr}\bigg|_{r=r_2}$ is the heat flux form the core to the outer sheet, and $q_w = \dfrac{2\pi r_1 h_2}{n} \left(T_1 - T_f \right)$ is the heat flux form the inner sheet to the air. Solving Eq. (6), the solution of the fluid temperature is

$$T_f \left(x \right) = Q / P + \left(T_0 - Q / P \right) e^{-Px} \tag{7}$$

where $Q = \dfrac{2\pi}{n \dot{m} c_p} \left(-\lambda_1 C_{12}^b + \lambda_3 C_{32}^b + h_c r_1 D_{21} \right)$, $P = \dfrac{2\pi}{n \dot{m} c_p} \left[-\lambda_1 C_{11}^b + \lambda_3 C_{31}^b + h_c r_1 \left(D_{11} - 1 \right) \right]$, and $D_{i1} = C_{i1}^a + C_{i1}^b \ln r$. Once T_f is obtained, the temperature distribution of the whole structure could be directly got by Eq. (4).

2.2 Effective thermal conductivity with effects of active cooling

Thermal conductivity is a key parameter used in calculating the temperature field of a structure and cellular metals possess relatively low thermal conductivities because of the special topologies of the prismatic cores compared with homo-metal materials. Meanwhile, less heat runs through the cellular metals caused by the heat transfer

between the metals and the low temperature fluid which means the active cooling. As a result, the effective thermal conductivity become much smaller by the effects of active cooling. The authors believe there is an innovative way to calculate the effective thermal conductivity with the effects of active cooling by treating the sandwich core as a 'black box' and assuming that the heat flux from the bottom sheet is equal to the heat flux from the core to the outer surface (q_2). In this way, the total heat flux from inner sheet dose not contain the heat taken away by the fluid medium and the effective thermal conductivity obtained by using this total heat flux includes the effect of active cooling. Based on the above assumption and the definition of the thermal conductivity, the effective thermal conductivity can be presented as

$$\bar{\lambda} = \int_{\mathrm{L}} \lambda(x)\,\mathrm{dx} = \int_{\mathrm{L}} \frac{\Delta q(x)}{\Delta T(x)/h_{\mathrm{c}}}\mathrm{dx} = \int_{\mathrm{L}} \frac{q_2(x)}{\left[T_3(r_2,x) - T_1(r_1,x)\right]/h_{\mathrm{c}}}\mathrm{dx} \tag{8}$$

In order to verify this assumption and the effective thermal conductivity obtained above, transient temperature changes of the sandwich structures are calculated by the theoretical method presented in [25, 26] and compared with the FE simulation, which are shown in section 4.1.

3 The thermal response of the structure

There would be a very high thermal response when a high temperature gradient exists on the structure. The structure will expand with the increasing temperature and there exists a certain level of thermo-mechanical interaction. In this paper, the influence of the structural deformation on the temperature field is ignored to simplify this problem. Moreover, it should be noticed that the computation model is a axial-symmetric cylindrical structure. After getting the temperature distribution, the structural thermal response based on the high-order displacement field theory is obtained.

3.1 The displacement field and the governing equation

The displacement field of the core can be expressed by the {2,1} displacement theory[27] and the sheets are represented by first-order shear deformation theory. The displacement field can be expressed as:

$$\begin{cases} \bar{u}_x^t = \left(u^a + u^d\right) - \left[z - \dfrac{h_f + h_c}{2}\right]\left(\dfrac{\partial w^a}{\partial x} + \dfrac{\partial w^d}{\partial x}\right) \\ \bar{u}_z^t = \left(w^a + w^d\right) \end{cases} \text{(for the top sheet)} \tag{9}$$

$$\begin{cases} \bar{u}_x^c = u^a + 2\dfrac{z}{h_c}u^d + h_f\dfrac{z}{h_c}\dfrac{\partial \bar{u}_z^c}{\partial x} \\ \bar{u}_z^c = w^a + 2\dfrac{z}{h_c}w^d + \left(1 - 4\dfrac{z^2}{h_c^2}\right)\phi \end{cases} \text{(for the core)} \tag{10}$$

and

$$\begin{cases} \bar{u}_x^t = \left(u^a - u^d\right) - \left[z + \dfrac{h_f + h_c}{2}\right]\left(\dfrac{\partial w^a}{\partial x} - \dfrac{\partial w^d}{\partial x}\right) \\ \bar{u}_z^t = \left(w^a - w^d\right) \end{cases} \text{ (for the bottom sheet)} \quad (11)$$

where

$$\begin{cases} \left\{u^a \quad w^a \quad \varphi_x^a\right\} = \dfrac{1}{2}\left\{\left(u^t + u^b\right) \quad \left(w^t + w^b\right) \quad \left(\varphi_x^t + \varphi_x^b\right)\right\} \\ \left\{u^d \quad w^d \quad \varphi_x^d\right\} = \dfrac{1}{2}\left\{\left(u^t - u^b\right) \quad \left(w^t - w^b\right) \quad \left(\varphi_x^t - \varphi_x^b\right)\right\} \end{cases} \quad (12)$$

where u^j and w^j $\left(j = t, b, c\right)$ are the displacement components on the middle surface of top sheet, bottom sheet and the core layer, φ_x^j is the rotations of a cross section in the $x-z$ plane of each layer, and ϕ is the displacement function describing the warping of the core that depends on the spatial position *x* within the middle plane of the core. The thermal stress - strain relationship has the form:

$$\begin{bmatrix} \sigma_x^i \\ \sigma_\theta^i \\ \sigma_z^i \\ \tau_{xz}^i \end{bmatrix} = \begin{bmatrix} C_{11}^i & C_{12}^i & C_{13}^i & 0 \\ C_{12}^i & C_{22}^i & C_{23}^i & 0 \\ C_{13}^i & C_{23}^i & C_{33}^i & 0 \\ 0 & 0 & 0 & C_{44}^i \end{bmatrix} \begin{bmatrix} \varepsilon_x^i - \alpha_x^i \Theta_i \\ \varepsilon_\theta^i - \alpha_\theta^i \Theta_i \\ \varepsilon_z^i - \alpha_z^i \Theta_i \\ \gamma_{xz}^i \end{bmatrix} \quad (13)$$

where Θ_i is the temperature change of the i^{th} layer of the structure, α_j^i ($j = x, \theta, z$ for the x, θ, z direction) is the coefficient of thermal expansion of the i^{th} layer of the structure, and

$$\begin{aligned} \boldsymbol{\varepsilon}^i &= \left\{\varepsilon_x^i \quad \varepsilon_\theta^i \quad \varepsilon_z^i \quad \gamma_{xz}^i\right\}^T \\ &= \left\{\frac{\partial \bar{u}_x^i(x,t)}{\partial x} \quad \frac{\bar{u}_z^i(x,t)}{R+z} \quad \frac{\partial \bar{u}_z^i(x,t)}{\partial z} \quad \frac{\partial \bar{u}_x^i(x,t)}{\partial z} + \frac{\partial \bar{u}_z^i(x,t)}{\partial x}\right\}^T \end{aligned} \quad (14)$$

$$\tilde{\boldsymbol{\varepsilon}}^i = \left\{\alpha_x^i \quad \alpha_\theta^i \quad \alpha_z^i \quad 0\right\}^T \Theta_i \quad (15)$$

The stress-strain relationship is generated by the homogenization method studied by Liu [18], Zhou [19] and Zhang[21].

The strain energy of the sandwich shell is

$$U = \frac{1}{2}\sum_i \int_V \left(\boldsymbol{\varepsilon}^i - \tilde{\boldsymbol{\varepsilon}}^i\right)^T \boldsymbol{\sigma}^i dV \quad (16)$$

Using Hamilton's variational principle, the governing equations are obtained as

$$\mathbf{Lu} = \mathbf{q} \quad (17)$$

where $\mathbf{L}$ is the matrix of partial differential operators, and the displacement vector is

$$\mathbf{u}=\left\{u^a \quad u^d \quad \varphi_x^a \quad \varphi_x^d \quad \phi \quad w^a \quad w^d\right\}^T \tag{18}$$

The forces $\mathbf{q}=\left\{q_1 \quad q_2 \quad q_3 \quad q_4 \quad q_5 \quad q_6 \quad q_7\right\}^T$ are:

$$\begin{cases} q_1=\tilde{N}_{x,x}^t+\tilde{N}_{x,x}^b+\tilde{N}_{x,x}^c; \quad q_2=\tilde{N}_{x,x}^t-\tilde{N}_{x,x}^b+\dfrac{2}{h_c}\tilde{M}_{x,x}^c; \\ q_3=\tilde{M}_{x,x}^t+\tilde{M}_{x,x}^b-\dfrac{h_f}{h_c}\tilde{M}_{x,x}^c; \quad q_4=\tilde{M}_{x,x}^t-\tilde{M}_{x,x}^b-\dfrac{h_f}{2}\tilde{N}_{x,x}^c; \\ q_5=\dfrac{4}{h_c^2}\tilde{P}_{x,x}^c-\tilde{N}_{x,x}^c; \\ q_6=-\dfrac{1}{R}\left(\tilde{N}_\theta^t+\tilde{N}_\theta^b+\tilde{N}_\theta^c\right); \\ q_7=-\dfrac{1}{R}\left(\tilde{N}_\theta^t-\tilde{N}_\theta^b+\dfrac{2}{h_c}\tilde{M}_\theta^c+\dfrac{2R}{h_c}\tilde{N}_z^c\right). \end{cases} \tag{19}$$

where $\tilde{N}$, $\tilde{M}$ and $\tilde{P}$ are the forces caused by the changing temperature. The details are given in Appendix I.

3.2 Solution

Simply supported boundary conditions at the two ends of the tube can be described as

$$at \quad x=0,L \qquad w^a=w^d=0, N_x{}^a=N_x{}^d=0, M_x{}^a=M_x{}^d=0 \tag{20}$$

where N and M are the shear force and the bending moment, and L is the length of the tube. The displacement vector is expressed in the form of Fourier series,

$$\begin{Bmatrix} u^a \\ u^d \\ \varphi_x^a \\ \varphi_x^d \\ \phi \\ w^a \\ w^d \end{Bmatrix}=\sum_{m=1}^{\infty}\begin{Bmatrix} \cos\left(\lambda_m x\right)U_m^a\left(t\right) \\ \cos\left(\lambda_m x\right)U_m^d\left(t\right) \\ \cos\left(\lambda_m x\right)\Phi_m^a\left(t\right) \\ \cos\left(\lambda_m x\right)\Phi_m^d\left(t\right) \\ \cos\left(\lambda_m x\right)\Phi_m^c\left(t\right) \\ \sin\left(\lambda_m x\right)W_m^a\left(t\right) \\ \sin\left(\lambda_m x\right)W_m^d\left(t\right) \end{Bmatrix} \tag{21}$$

where $\lambda_m=m\pi/L$.

The thermal stress of each layer is

$$\left\{\tilde{\sigma}_{x,t}^i \quad \tilde{\sigma}_{\theta,t}^i \quad \tilde{\sigma}_{z,t}^i\right\}=\sum_{m=1}^{\infty}\left\{\Sigma_{x,m}^i \quad \Sigma_{\theta,m}^i \quad \Sigma_{z,m}^i\right\}\sin\left(\lambda_m x\right) \tag{22}$$

Each of the above Fourier series can be written as:

$$\Sigma_{j,m}^{i} = \frac{2}{L}\int_0^L \tilde{\sigma}_j^i \sin\left(\lambda_m x\right) dx = \frac{2}{L}\int_0^L \beta_j^i \Theta_i\left(z,t\right)\sin\left(\lambda_m x\right) dx, \quad j = x,\theta,z; \quad i = t,c,b \tag{23}$$

where

$$\begin{bmatrix} \beta_x^i \\ \beta_\theta^i \\ \beta_z^i \end{bmatrix} = \begin{bmatrix} C_{11}^i & C_{12}^i & C_{13}^i \\ C_{12}^i & C_{22}^i & C_{23}^i \\ C_{13}^i & C_{23}^i & C_{33}^i \end{bmatrix} \begin{bmatrix} \alpha_x^i \\ \alpha_\theta^i \\ \alpha_z^i \end{bmatrix} \tag{24}$$

and $\Theta_i\left(z,t\right)$ is the temperature change of each layer. Introducing Eqs. (21) and (22) into Eq. (17) results in seven algebraic equations in which the trigonometric functions are factored out, leaving only the amplitudes U_m^a, U_m^d, Φ_m^a, Φ_m^d, Φ_m^c, W_m^a and W_m^d as unknowns. The stiffness matrix and the thermal force vector are shown in Appendices II and III. Once the displacement amplitudes are determined, the displacements are then computed in a straightforward manner from Eqs. (9)-(11) and (21). Then stress and strain of each layer are obtained.

4 Results and discussion

In this section, the temperature changes from the theoretical method and the FE simulation are analyzed and compared. The thermal structural responses are calculated after getting the temperature field based on the discussion in section 3. The thermal displacement, stress and strain of the tubes with the Square and Kagome cores are compared with the results from the FE simulation. In the last part of this section, the advantages of active heat dissipation are discussed and the improvements of the structural response are explained.

In this paper, it is assumed that all components of the sandwich tubes are made of 4340 steel which Young's modulus E = 193GPa, density ρ = 8000kg·m^{-3}, Poisson's ratio ν =0.25, yield stress σ_y = 792MPa, mean thermal expansion α =12ppm·ºC^{-1}, specific heat capacity of solids c = 475J·(kg·ºC)$^{-1}$, and thermal conductivity k = 44.5 W·(m·ºC)$^{-1}$. The density of the air ρ_{f} =1.29 kg·m^{-3} and the specific of the air c_{p} =1030 J·(kg·ºC)$^{-1}$. The heat transfer coefficients H_{a} =530W·(m^2·ºC)$^{-1}$ and H_{b} = 10W·(m^2·ºC)$^{-1}$. The fluid velocity v_0 =1m·s^{-1} and the initial temperature of solids and fluid is the 20ºC. The inner sheets of the tubes are subjected to the hot air which temperature is 400ºC. The dimensional and material parameters of the sandwich tubes with Square and Kagome cores are shown in Table 2. Based on the discussion in

section 2, the effective conductivities considering the heat transfer between the solid and fluid is also shown in Table 2. The stiffness parameters of the sandwich cores obtained by the homogenization method are shown in Table 3.

Table 2 Material parameters of the sandwich tubes

	Face sheet	Core (Square)	Core (Kagome)
Thickness (mm)	10	40	40
Effective Conductivity (without considering active cooling $W\cdot(m\cdot^oC)^{-1}$)	44.5	2.6787	4.1116
Effective Conductivity (considering active cooling, $W\cdot(m\cdot^oC)^{-1}$)	44.5	0.0801	0.1729
Density (kg·m-3)	8000	957.6	1607.2

Inner radius: a=0.14m, outer radius: b=0.2m.

Table 3 The stiffness parameters of cores of the sandwich tubes

	c_{11}	c_{12}	c_{13}	c_{22}	c_{23}	c_{33}	c_{44}
Square	42.79	7.03	2.81	30.56	0	12.23	0.25
Kagome	78.09	15.05	2.90	56.68	8.79	3.83	0.97

4.1 Comparison of the transient temperature field between analytical results and FE simulations

The temperature changes obtained by the theoretical solution and the FE simulations are compared to verify the correction of the effective thermal conductivity obtained in Eq. (8). The bottom sheet, the middle of the core, and the top sheet of sandwich tubes with Square and Kagome cores are selected. The FE simulations are carried out by the commercial software ABAQUS/CFD. Due to the computation model is a axial-symmetric cylindrical structure, a unit cell (1/32 part) of the whole structure is used for the FE simulations. In the heat transfer analysis, the 20-node quadratic heat transfer brick (DC3D20) is used for the solid and the 8-node linear fluid brick (FC3D8) is used for the fluid. The 20-node quadratic brick, reduced integration (C3D20R) is used for the solid's thermal-response analysis. The temperature of whole structure are shown in Fig. 3(a) and Fig.4(a), and the temperature of the air (fluid) are shown in Fig.3 (b) and Fig.4 (b).

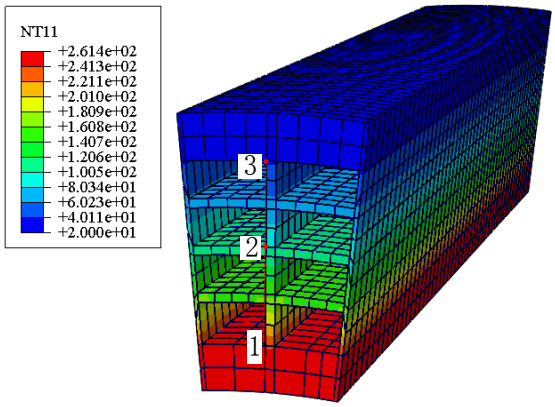

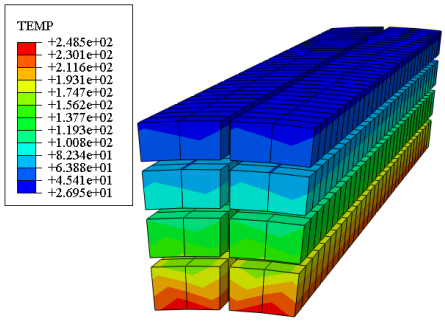

(a) The temperature of the tube with Square core (b) The temperature of the fluid in Square core

Fig. 3 the temperature of the tube with Square core and fluid

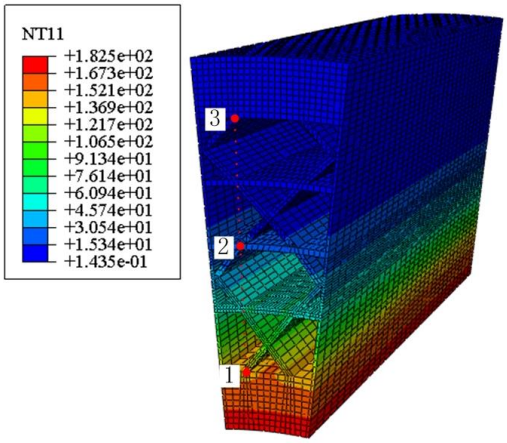

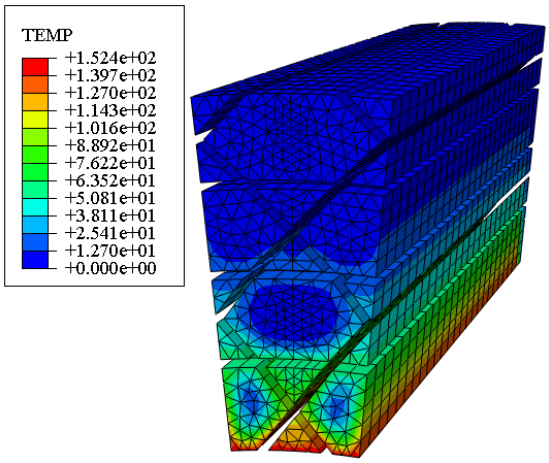

(a) The temperature of the tube with Kagome core (b) The temperature of the fluid in Kagome core

Fig. 4 the temperature of the tube with Kagome core and fluid

Three points are selected which is in the Bottom sheet of the entrance cross-section of the fluid (Point 1), middle of the core (Point 2) and the top sheet (Point 3) to compare with the theoretical results. The temperature changes considering active heat dissipation are plotted in solid and hollow dot curves in Fig. 5 and Fig. 6, which represent analytical solutions and FE simulations. It can be seen that the analytical results are very close to the FE results and they have the same trend in the time-domain, which reveals that the effective thermal conductivity with active heat dissipation is correct and the method is capable of predicating the transient temperature distribution along the radial direction efficiently. Compared with the tube with the Square core, the temperature of the tube with the Kagome core increases slowly and the top sheet and the middle of the core layer develop a very low and slow changing temperature field. This means that the sandwich tube with Kagome core has a better heat dissipation capability and a relatively lower effective heat conductivity

which can reduce the heat flux from the high temperature to the low temperature region.

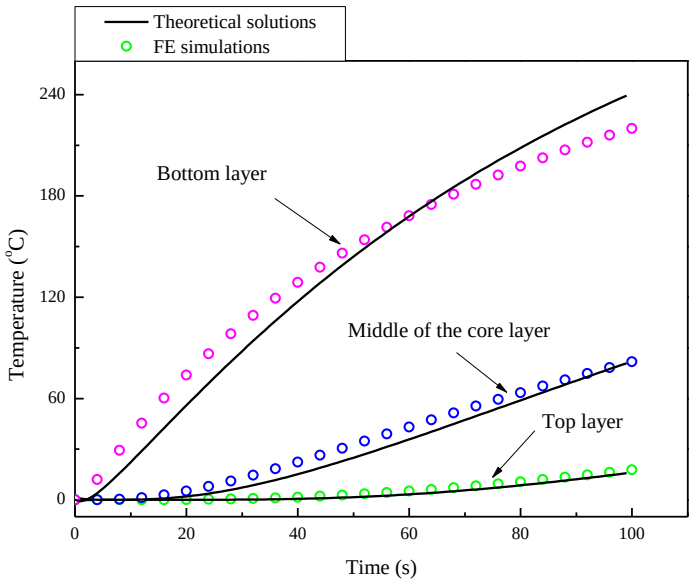

Fig. 5 The transient temperature of the sandwich tube with the Square core

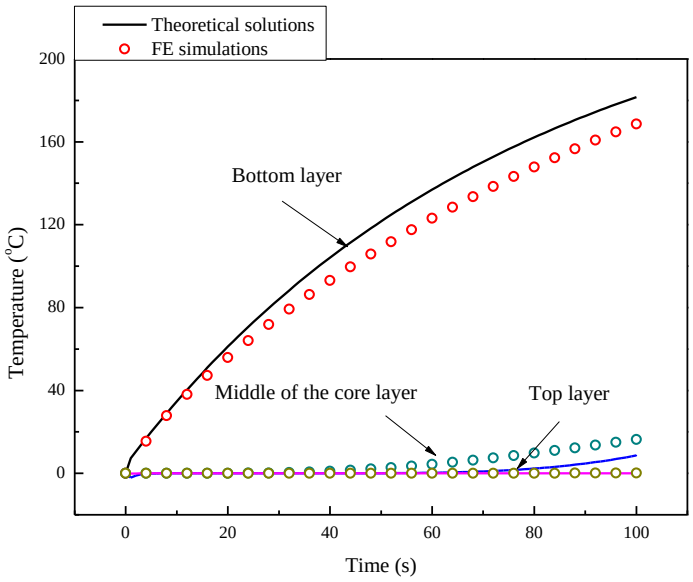

Fig. 6 The transient temperature of sandwich tube with the Kagome core

4.2 Thermal response

The structural responses of sandwich tubes with Square and Kagome cores subjected to the thermal loads are studied in this section. The displacements and stresses caused by the changing temperature are calculated. The results of theoretical method and the FE simulation are also compared in this section.

As shown in Fig. 7 and Fig. 8, the distributions of the radial displacements in

sandwich tubes with Square and Kagome cores demonstrate that the theoretical results are in good agreement with the results of FE simulations. Moreover, the theoretical results are a little bigger than the results of FE simulations in the bottom sheet, but this relation reverses in the top sheet. It is confirmed that the theoretical solution considering active heat dissipation has the ability of obtaining reliable displacements caused by the changing temperature.

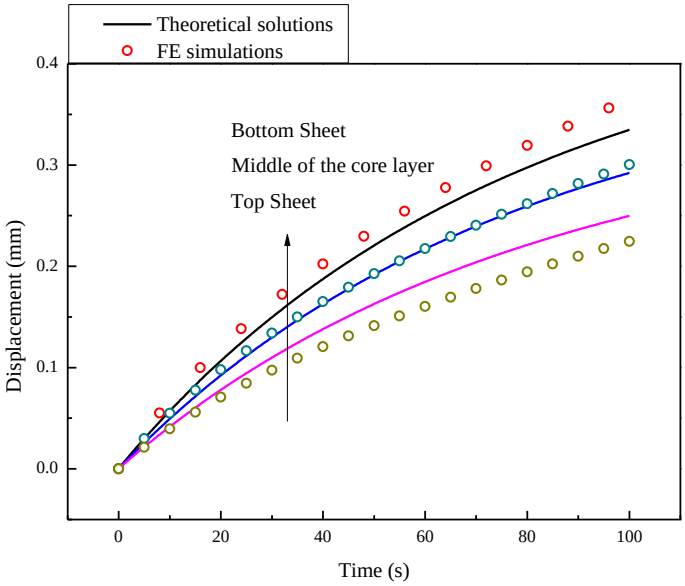

Fig. 7 The transient displacements of the sandwich tube with the Square core

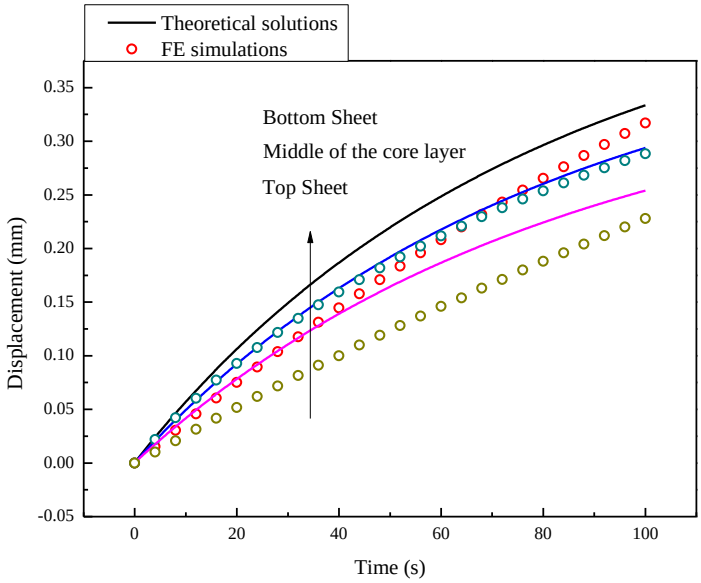

Fig. 8 The transient displacements of the sandwich tube with the Kagome core

The amplitudes of the radial, hoop and axial stresses of the sandwich tubes with Square and Kagome cores obtained by the theoretical solution and the FE simulations

are shown in Fig. 9 to Fig. 14. For the square core, the radial stress of the bottom sheet is bigger than that of the top sheet and the middle of the core layer, and the same phenomenon appears for the hoop and axial stresses. Moreover, it should be noticed that the hoop stress is bigger than the radial and axial stresses, which shows the important role of the hoop stress in the axial-symmetric cylindrical structure, and the similar trend is also found in the tube with Kagome core.

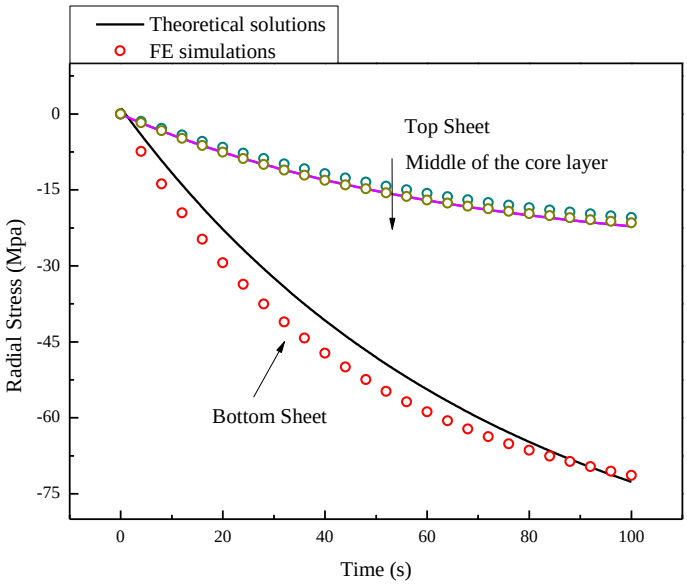

Fig. 9 Radial Stress of the sandwich tube with the Square core

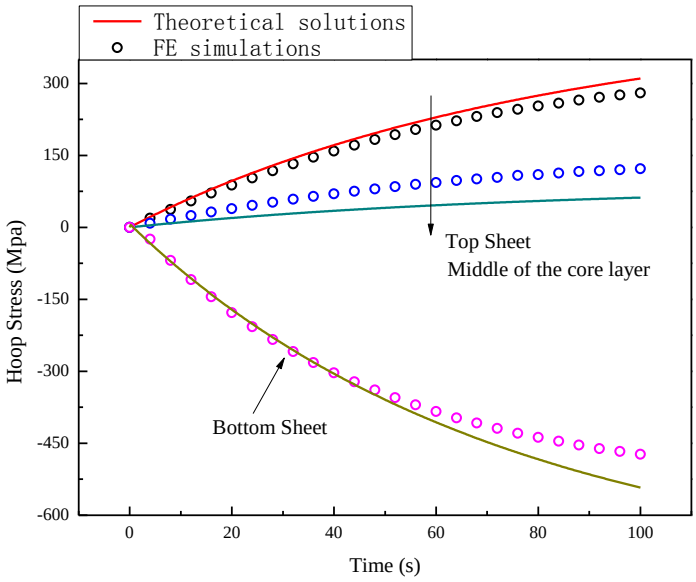

Fig. 10 Hoop Stress of the sandwich tube with the Square core

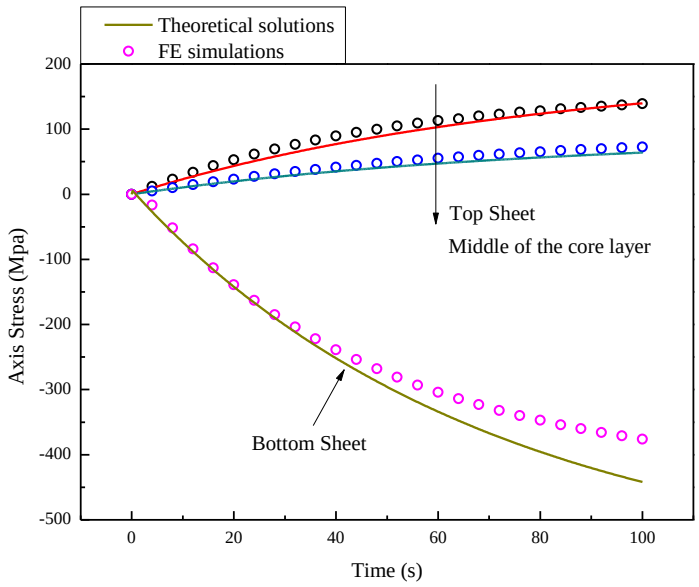

Fig. 11 Axial Stress of the sandwich tube with the Square core

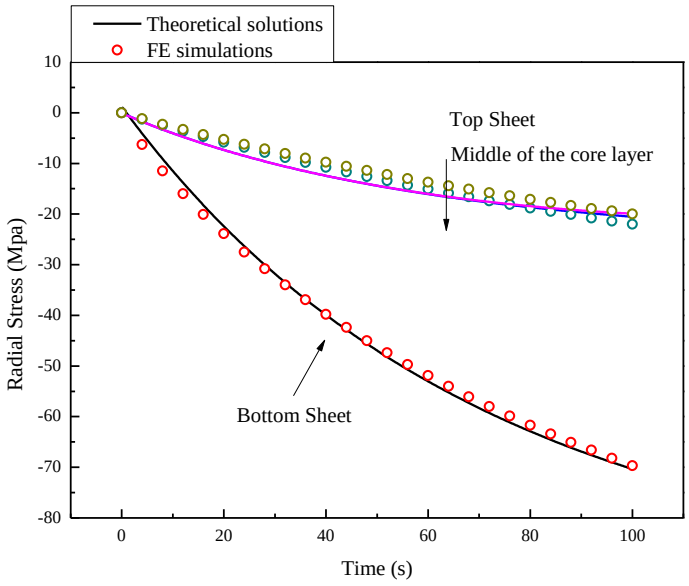

Fig. 12 Radial Stress of the sandwich tube with the Kagome core

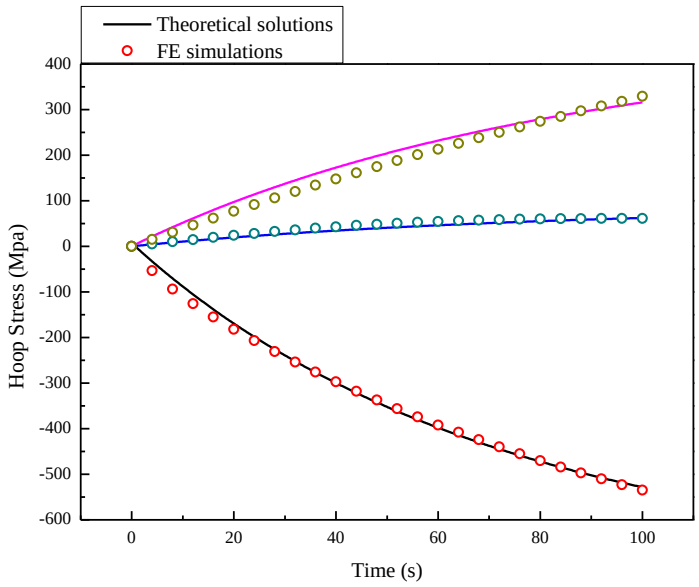

Fig. 13 Hoop Stress of the sandwich tube with the Kagome core

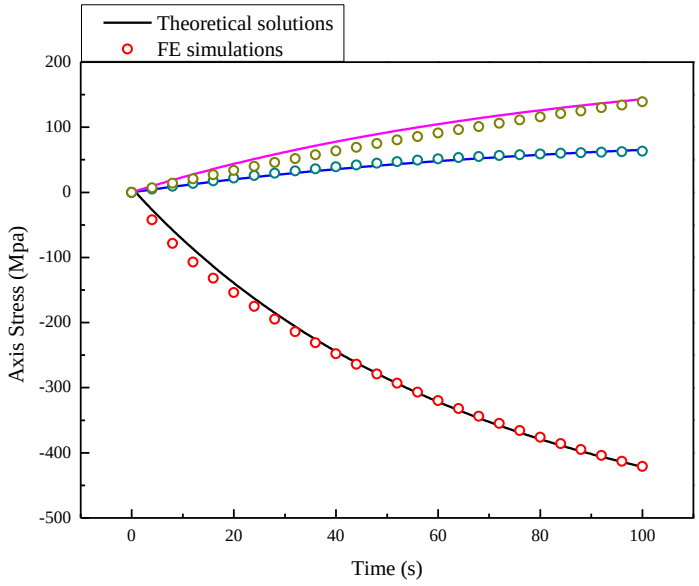

Fig. 14 Axial Stress of the sandwich tube with the Kagome core

The good agreement between theoretical results and FE results indicates that the high-order displacement theory considering the thermal effects is capable of accurately predicting the thermal response of sandwich tubes with prismatic cores. Based on the above results, it is found that a big thermal stress appears when a large temperature gradient is applied onto the structure. Active cooling capability of the cellular materials could reduce the thermal response and the stress magnitude of the structure, which will be discussed in section 4.3.

4.3 Reduction of the thermal response by active heat dissipation

As found in previous studies, one attractive advantage of the prismatic cellular materials is the active cooling, which have the capability of transferring and taking away heat by the fluid medium forced though the open hole. In recent decades, many researchers have focused on the heat dissipation of prismatic cellular materials as a cooling panel and the optimization of structures to adapt to different conditions. However, few researchers have dealt with the thermal response of sandwich tubes with prismatic cores and the effects of active cooling on the stress distribution. In this section, the effects of active cooling are analyzed by using the effective thermal conductivities listed in Table 2 . The reduction of the thermal displacements, hoop stress and axial stress by considering active cooling are discussed and the percentage reduction of the maximum stresses with different number of revolving periodic unit cells are also analyzed. The percentage reduction of the radial displacement of the sandwich tubes with Square and Kagome cores are shown in Fig. 15. Apparently, the effects of active cooling on the radial displacement gradually weaken along the radius. The percentage reduction becomes bigger with time, which means a strong influence of active cooling.

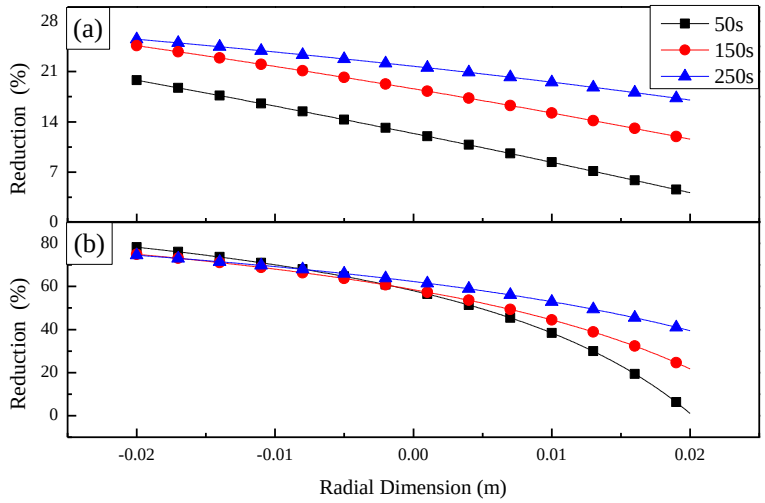

Fig. 15 Reduction on the radial displacement of the sandwich tube with the (a) Square and (b) Kagome core

The percentage reductions of the hoop stresses of the bottom and top sheets in sandwich tubes with Square and Kagome cores are compared in Fig. 16. It can be seen that the effects of active cooling become greater as time advances. At the 150^{th} second, the percentage reduction in the stress is bigger than that at the 50^{th} second and the same phenomenon can be observed between the 150^{th} seconds and the 250^{th} seconds. The reduction of the hoop stress in the top sheet does not change much in the radial direction, while the percentage reduction of the hoop stress in the bottom sheet becomes bigger along the radius except at the 250^{th} seconds. In comparison, the sandwich tube with Kagome core has a bigger reduction in the stress at all time.

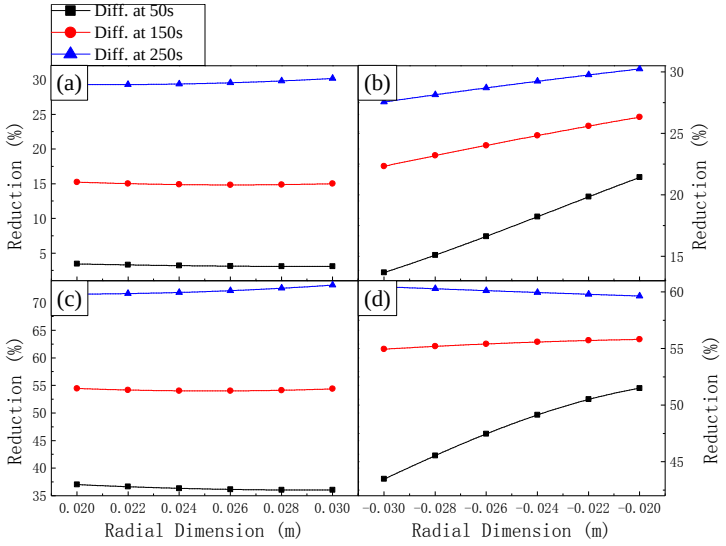

Fig. 16 Reduction on the hoop stress of (a) the top sheet of the sandwich tube with the Square core (b) the bottom sheet of the sandwich tube with the Square core (c) the top sheet of the sandwich tube with the Kagome core and(d)the bottom sheet of the sandwich tube with the Kagome core

In the design of hollow sandwich tubes with prismatic cores, a different number of the unit cell in the circumferential direction results in a different sandwich structure and it will have a different structural response. Table 4 and Table 5 make the comparisons of the structural responses of the tubes which have 28, 30, 32, 34, 36, 38 and 40 periodic unit cells in their sections. For the tube with a Square core, the percentage reductions of the structural responses increase with the number of the unit cells and the hoop stress of the inner and middle of the core are much smaller when active heat dissipation is considered. A similar trend is also found in the analysis of the tube with the Kagome core, which shows a growing percentage reduction of all the thermal responses with the increase of the number of the unit cells except the radial displacement. It should be noticed that the comparisons demonstrate the effects of active cooling only (but not necessarily the stress decrease with the increase of the divisional parts).

Table 4 The percentage reduction of the sandwich tube with the Square core

Parts	Radial displacement			Radial stress		
	Bottom sheet	Middle of the core	Top sheet	Bottom of the core	Middle of the core	Top of the core
28	10.2	5.4	0.9	30.5	3.1	72.1
30	10.7	5.7	0.8	31.9	3.4	73.0
32	11.2	6.1	0.6	33.3	3.8	73.8
34	11.6	6.4	0.6	34.6	4.2	74.5
36	12.1	6.7	0.8	36.0	4.7	75.1

38	12.6	7.1	1.0	37.3	5.2	75.7
40	13.0	7.4	1.2	38.6	5.7	76.2

	Hoop stress			Axial stress		
Parts	Bottom sheet	Middle of the core	Top sheet	Bottom sheet	Middle of the core	Top sheet
28	25.4	69.4	31.7	38.3	45.0	3.3
30	26.6	72.7	32.5	39.7	46.3	4.1
32	27.8	75.9	33.4	41.0	47.5	4.8
34	28.9	78.9	34.2	42.3	48.5	5.6
36	30.0	81.7	35.1	43.6	49.5	6.4
38	31.1	84.5	35.9	44.8	50.3	7.2
40	32.2	87.1	36.8	46.0	51.1	8.0

Table 5 The percentage reduction of the sandwich tube with Kagome core

	Radial displacement			Radial stress		
Parts	Bottom sheet	Middle of the core	Top sheet	Bottom of the core	Middle of the core	Top of the core
28	29.5	10.9	36.9	77.5	10.5	67.7
30	28.8	10.3	36.4	80.6	11.1	66.9
32	28.1	9.7	36.0	83.5	11.6	66.4
34	27.4	9.1	35.7	86.0	12.0	66.4
36	26.9	8.6	35.5	88.0	12.3	67.1
38	26.5	8.2	35.3	88.9	12.7	69.1
40	26.6	8.1	35.2	86.2	15.3	74.6

	Hoop stress			Axial stress		
Parts	Bottom sheet	Middle of the core	Top sheet	Bottom sheet	Middle of the core	Top sheet
28	61.2	80.6	65.1	25.2	49.7	55.9
30	61.9	81.7	67.2	24.3	51.4	55.0
32	62.6	82.5	69.3	23.5	52.8	54.2
34	63.1	83.2	71.5	22.9	54.0	53.3
36	63.5	83.8	73.8	22.6	54.8	52.4
38	63.7	84.0	76.1	22.9	55.1	51.4
40	63.1	83.4	78.3	25.1	52.4	50.5

5. Conclusions

Hollow cylindrical tubes with prismatic cores are analyzed in this paper. The section of the tube is divided by a number of revolving periodic unit cells whose topologies of unit cells are either Square or Kagome. The effective thermal conductivity considering active heat dissipation is derived and verified by comparing the results between the analytical solution and the FE simulation. The results demonstrate that

the method could obtain the correct effective thermal conductivity, which covers the effects of active heat dissipation, for predicating the transient temperature. After getting the transient temperature field, the thermal structural response is obtained by the high-order sandwich model and a series of FE simulations are carried out to verify the analytical results. The comparisons demonstrate that the method of obtaining the effective thermal conductivity and the high-order displacement theory can provide reliable results of the structural responses. The effects of active heat dissipation for reducing the thermal responses of the sandwich tubes are studied by comparing the results between cases with active heat dissipation and without it, which shows a remarkable advantage of the prismatic cellular metals. A series of models which contain 28, 30, 32, 34, 36, 38 and 40 periodic unit cells in their sandwich cores are analyzed. The hoop stresses of the inner and middle of the core are found to be much smaller when active heat dissipation is considered. The percentage reductions of all the thermal responses of structure with Kagome core also grow with the increase of the number of unit cells except the radial displacement. The thermal loads resulted from temperature gradients in the sandwich tube cause large thermal stresses, which are harmful to the structure and its reliability. Therefore, the multifunctional design of the sandwich tube with prismatic cores is in urgent need, for engine combustors under extremely hostile conditions. The work presented in this paper can be used in designing metallic sandwich tubes with prismatic cores for more applicability.

Appendix I

$$\left\{\tilde{N}_x^b \quad \tilde{M}_x^b \quad \tilde{N}_\theta^b\right\} = \int_{-\frac{h_c}{2}-h_f}^{-\frac{h_c}{2}} \left\{\tilde{\sigma}_x^b\left(1+\frac{z}{R}\right) \quad \tilde{\sigma}_x^b\left(1+\frac{z}{R}\right)\left(z+\frac{h_c+h_f}{2}\right) \quad \tilde{\sigma}_\theta^b\right\} dz$$

$$\left\{\tilde{N}_x^t \quad \tilde{M}_x^t \quad \tilde{N}_\theta^t\right\} = \int_{\frac{h_c}{2}}^{\frac{h_c}{2}+h_f} \left\{\tilde{\sigma}_x^t\left(1+\frac{z}{R}\right) \quad \tilde{\sigma}_x^t\left(1+\frac{z}{R}\right)\left(z-\frac{h_c+h_f}{2}\right) \quad \tilde{\sigma}_\theta^t\right\} dz$$

$$\left\{\tilde{N}_x^c \quad \tilde{M}_x^c \quad \tilde{P}_x^c \quad \tilde{N}_\theta^c \quad \tilde{M}_\theta^c \quad \tilde{N}_z^c\right\}$$

$$= \int_{-\frac{h_c}{2}}^{\frac{h_c}{2}} \left\{\tilde{\sigma}_x^c\left(1+\frac{z}{R}\right) \quad \tilde{\sigma}_x^c z\left(1+\frac{z}{R}\right) \quad \tilde{\sigma}_x^c z^2\left(1+\frac{z}{R}\right) \quad \tilde{\sigma}_\theta^c \quad \tilde{\sigma}_\theta^c z \quad \tilde{\sigma}_z^c\left(1+\frac{z}{R}\right)\right\} dz$$

Appendix II

The element of the stiffness matrix are defined

$$K_{11} = -\lambda_m^2\left(2C_{11}^f h_f + C_{11}^c h_c\right);$$

$$K_{12} = K_{21} = -\lambda_m^2\left(2\Lambda C_{11}^f h_f + C_{11}^c \frac{h_c^2}{6R}\right);$$

$$K_{13} = K_{31} = K_{24} = K_{42} = -\lambda_m^2\left(2C_{11}^f h_f^2 - C_{11}^c h_c^2\right)\frac{h_f}{12R};$$

$$K_{14} = K_{41} = \frac{1}{2}\lambda_m^2 C_{11}^c h_f h_c \;;$$

$$K_{15} = K_{51} = \frac{2}{3}\lambda_m^2 C_{11}^c h_c \;;$$

$$K_{16} = K_{61} = \lambda_m \left(2C_{12}^f \frac{h_f}{R} + C_{12}^c \frac{h_c}{R} \right);$$

$$K_{17} = K_{71} = 2\lambda_m C_{13}^c \;;$$

$$K_{22} = -\lambda_m^2 \left(2C_{11}^f h_f + \frac{1}{3} C_{11}^c h_c \right) - \frac{4}{h_c}\kappa_c^2 C_{44}^c \;;$$

$$K_{23} = K_{32} = \frac{1}{6}\lambda_m^2 C_{11}^c h_f h_c + 2\frac{h_f}{h_c}\kappa_c^2 C_{44}^c \;;$$

$$K_{25} = K_{52} = \lambda_m^2 C_{11}^c \frac{h_c^2}{15R} - \frac{4}{3R}\kappa_c^2 C_{44}^c \;;$$

$$K_{26} = K_{62} = -2\lambda_m \kappa_c^2 C_{44}^c \;;$$

$$K_{27} = K_{72} = \lambda_m \left[2C_{12}^f \frac{h_f}{R} + \left(C_{12}^c + C_{13}^c - \kappa_c^2 C_{44}^c \right) \frac{h_c}{3R} \right];$$

$$K_{33} = -\frac{1}{12}\lambda_m^2 \left(2C_{11}^f h_f + C_{11}^c h_c \right) h_f^2 - \left(2\kappa_f^2 C_{44}^f + \kappa_c^2 C_{44}^c \frac{h_f}{h_c} \right) h_f \;;$$

$$K_{34} = K_{43} = -\lambda_m^2 \left(4\Lambda C_{11}^f h_f R + C_{11}^c h_c^2 \right) \frac{h_f^2}{24R} - 2\Lambda \kappa_f^2 C_{44}^f h_f \;;$$

$$K_{35} = K_{53} = -\lambda_m^2 C_{11}^c \frac{h_f h_c^2}{30R} + \kappa_c^2 C_{44}^c \frac{2h_f}{3R} \;;$$

$$K_{36} = K_{63} = \lambda_m \left(\kappa_c^2 C_{44}^c - 2\kappa_f^2 C_{44}^f \right) h_f \;;$$

$$K_{37} = K_{73} = \lambda_m \left[-12\Lambda \kappa_f^2 C_{44}^f R + h_c \left(\kappa_c^2 C_{44}^c - C_{12}^c - C_{13}^c \right) \right] \frac{h_f}{6R} \;;$$

$$K_{44} = -\frac{1}{12}\lambda_m^2 \left(2C_{11}^f h_f + 3C_{11}^c h_c \right) h_f^2 - 2\kappa_f^2 C_{44}^f h_f \;;$$

$$K_{45} = K_{54} = -\frac{1}{3}\lambda_m^2 C_{11}^c h_f h_c \;;$$

$$K_{46}=K_{64}=-\lambda_m\left(4\Lambda\kappa_f^2C_{44}^fR+C_{12}^ch_c\right)\frac{h_f}{2R};$$

$$K_{47}=K_{74}=-\lambda_m\left(2\kappa_f^2C_{44}^f+C_{13}^c\right)h_f;$$

$$K_{55}=-\frac{8}{15}\lambda_m^2C_{11}^ch_c-\frac{16}{3h_c}\kappa_c^2C_{44}^c;$$

$$K_{56}=K_{65}=-\lambda_m\left(\kappa_c^2C_{44}^c+C_{12}^c\right)\frac{2h_c}{3R};$$

$$K_{57}=K_{75}=-\frac{4}{3}\lambda_m\left(\kappa_c^2C_{44}^c+C_{13}^c\right);$$

$$K_{66}=-\lambda_m^2\left(2\kappa_f^2C_{44}^fh_f+\kappa_c^2C_{44}^ch_c\right)-\frac{1}{R}\left(g_1^tC_{22}^f+g_1^bC_{22}^f+g_1^cC_{22}^c\right);$$

$$K_{67}=K_{76}=-\lambda_m^2\left(2\Lambda\kappa_f^2C_{44}^fh_f+\kappa_c^2C_{44}^c\frac{h_c^2}{6R}\right)-\frac{1}{R}\left(g_1^tC_{22}^f-g_1^bC_{22}^f+\frac{2g_2^c}{h_c}C_{22}^c+2C_{23}^c\right);$$

$$K_{77}=-\frac{1}{3}\lambda_m^2\left(6\kappa_f^2C_{44}^fh_f+\kappa_c^2C_{44}^ch_c\right)-\frac{1}{R}\left(g_1^tC_{22}^f+g_1^bC_{22}^f+\frac{2g_3^c}{h_c^2}C_{22}^c+\frac{4R}{h_c}C_{33}^c\right);$$

Where, C_{ij}^f and C_{ij}^c are the stiffness confections of the upper and bottom sheets and core, $C_{ij}^t=C_{ij}^b=C_{ij}^f$

The correction confection of the sheets and core are $\kappa_f=5/6$ and $\kappa_c=1$. $R=(a+b)/2$ is the mean redial. Λ and $g_j^i,\ j=1,2,3$ are

$$\Lambda=\frac{h_c+h_f}{2R},\quad g_1^t=\ln\left(\frac{1+\frac{h_c+2h_f}{2R}}{1+\frac{h_c}{2R}}\right),g_1^b=\ln\left(\frac{1-\frac{h_c}{2R}}{1-\frac{h_c+2h_f}{2R}}\right),g_1^c=\ln\left(\frac{1+\frac{h_c}{2R}}{1-\frac{h_c}{2R}}\right),$$

$g_2^c=h_c-Rg_1^c$, $g_3^c=R^2g_1^c-Rh_c$.

Appendix III

The thermal force $\mathbf{f}_m$ can be written as

$$f_1=-\frac{2}{L}(1-\cos m\pi)\left[\beta_x^f\int_{-\frac{h_c}{2}-h_f}^{-\frac{h_c}{2}}\Theta_b\left(1+\tfrac{z}{R}\right)dz+\beta_x^c\int_{-\frac{h_c}{2}}^{\frac{h_c}{2}}\Theta_c\left(1+\tfrac{z}{R}\right)dz+\beta_x^f\int_{\frac{h_c}{2}}^{\frac{h_c}{2}+h_f}\Theta_t\left(1+\tfrac{z}{R}\right)dz\right]$$

$$f_2=-\frac{2}{L}\left(1-\cos m\pi\right)\left[-\beta_x^f\int_{-\frac{h_c}{2}-h_f}^{-\frac{h_c}{2}}\Theta_b\left(1+\tfrac{z}{R}\right)dz+\tfrac{2}{h_c}\beta_x^c\int_{-\frac{h_c}{2}}^{\frac{h_c}{2}}\Theta_c\left(1+\tfrac{z}{R}\right)zdz+\beta_x^f\int_{\frac{h_c}{2}}^{\frac{h_c}{2}+h_f}\Theta_t\left(1+\tfrac{z}{R}\right)dz\right]$$

$$f_3=-\frac{2}{L}\left(1-\cos m\pi\right)\left[\beta_x^f\int_{-\frac{h_c}{2}-h_f}^{-\frac{h_c}{2}}\Theta_b\left(z+\Lambda R\right)\left(1+\tfrac{z}{R}\right)dz-\tfrac{h_f}{h_c}\beta_x^c\int_{-\frac{h_c}{2}}^{\frac{h_c}{2}}\Theta_c\left(1+\tfrac{z}{R}\right)zdz\right.$$
$$\left.+\beta_x^f\int_{\frac{h_c}{2}}^{\frac{h_c}{2}+h_f}\Theta_t\left(z-\Lambda R\right)\left(1+\tfrac{z}{R}\right)dz\right]$$

$$f_4=-\frac{2}{L}\left(1-\cos m\pi\right)\left[-\beta_x^f\int_{-\frac{h_c}{2}-h_f}^{-\frac{h_c}{2}}\Theta_b\left(z+\Lambda R\right)\left(1+\tfrac{z}{R}\right)dz-\tfrac{h_f}{2}\beta_x^c\int_{-\frac{h_c}{2}}^{\frac{h_c}{2}}\Theta_c\left(1+\tfrac{z}{R}\right)dz\right.$$
$$\left.+\beta_x^f\int_{\frac{h_c}{2}}^{\frac{h_c}{2}+h_f}\Theta_t\left(z-\Lambda R\right)\left(1+\tfrac{z}{R}\right)dz\right]$$

$$f_5=-\frac{2}{L}\left(1-\cos m\pi\right)\left[\tfrac{4}{h_c^2}\beta_x^c\int_{-\frac{h_c}{2}}^{\frac{h_c}{2}}\Theta_c\left(1+\tfrac{z}{R}\right)z^2dz-\beta_x^c\int_{-\frac{h_c}{2}}^{\frac{h_c}{2}}\Theta_c\left(1+\tfrac{z}{R}\right)dz\right]$$

$$f_6=\frac{2}{LR\lambda_m}\left(1-\cos m\pi\right)\left[\beta_\theta^f\int_{-\frac{h_c}{2}-h_f}^{-\frac{h_c}{2}}\Theta_b dz+\beta_\theta^c\int_{-\frac{h_c}{2}}^{\frac{h_c}{2}}\Theta_c dz+\beta_\theta^f\int_{\frac{h_c}{2}}^{\frac{h_c}{2}+h_f}\Theta_t dz+\left(R-\tfrac{h_c+2h_f}{2}\right)p(t)\right]$$

$$f_7=\frac{2}{LR\lambda_m}\left(1-\cos m\pi\right)\left[-\beta_\theta^f\int_{-\frac{h_c}{2}-h_f}^{-\frac{h_c}{2}}\Theta_b dz+\tfrac{2}{h_c}\beta_\theta^c\int_{-\frac{h_c}{2}}^{\frac{h_c}{2}}\Theta_c zdz+\tfrac{2R}{h_c}\beta_z^c\int_{-\frac{h_c}{2}}^{\frac{h_c}{2}}\Theta_c\left(1+\tfrac{z}{R}\right)dz\right.$$
$$\left.+\beta_\theta^f\int_{\frac{h_c}{2}}^{\frac{h_c}{2}+h_f}\Theta_t dz-\left(R-\tfrac{h_c+2h_f}{2}\right)p(t)\right]$$

where the expansion coefficients of each sheet are $\beta_j^t=\beta_j^b=\beta_j^f,\ j=x,\theta,z$

$$\left\{\tilde{N}_x^b\quad\tilde{M}_x^b\quad\tilde{N}_\theta^b\right\}=\int_{-\frac{h_c}{2}-h_f}^{-\frac{h_c}{2}}\left\{\tilde{\sigma}_x^b\left(1+\frac{z}{R}\right)\quad\tilde{\sigma}_x^b\left(1+\frac{z}{R}\right)\left(z+\frac{h_c+h_f}{2}\right)\quad\tilde{\sigma}_\theta^b\right\}dz$$

$$\left\{\tilde{N}_x^t\quad\tilde{M}_x^t\quad\tilde{N}_\theta^t\right\}=\int_{\frac{h_c}{2}}^{\frac{h_c}{2}+h_f}\left\{\tilde{\sigma}_x^t\left(1+\frac{z}{R}\right)\quad\tilde{\sigma}_x^t\left(1+\frac{z}{R}\right)\left(z-\frac{h_c+h_f}{2}\right)\quad\tilde{\sigma}_\theta^t\right\}dz$$

$$\left\{\tilde{N}_x^c\quad\tilde{M}_x^c\quad\tilde{P}_x^c\quad\tilde{N}_\theta^c\quad\tilde{M}_\theta^c\quad\tilde{N}_z^c\right\}$$
$$=\int_{-\frac{h_c}{2}}^{\frac{h_c}{2}}\left\{\tilde{\sigma}_x^c\left(1+\frac{z}{R}\right)\quad\tilde{\sigma}_x^c z\left(1+\frac{z}{R}\right)\quad\tilde{\sigma}_x^c z^2\left(1+\frac{z}{R}\right)\quad\tilde{\sigma}_\theta^c\quad\tilde{\sigma}_\theta^c z\quad\tilde{\sigma}_z^c\left(1+\frac{z}{R}\right)\right\}dz$$

where the $\tilde{\boldsymbol{\sigma}}^i$ is the thermal stress

$$\tilde{\boldsymbol{\sigma}}^i=\mathbf{D}^i\tilde{\boldsymbol{\varepsilon}}^i,\quad\tilde{\boldsymbol{\sigma}}^i=\left\{\tilde{\sigma}_x^i\quad\tilde{\sigma}_\theta^i\quad\tilde{\sigma}_z^i\quad 0\right\}^T$$

Acknowledgements

The authors wish to thank the National Basic Research Program of China (2011CB610300), the National Natural Science Foundation of China (11172239), the Doctoral Program Foundation of Education Ministry of China (20126102110023) and

the Open Foundation of State Key Laboratory of Structural analysis of Industrial Equipment (GZ0802).

References

1. Roy, G.D., Frolov, S.M., Borisov, A.A., et al.: Pulse detonation propulsion: challenges, current status, and future perspective. Prog. Energ. Combust. **30**, 545-672 (2004).
2. Hosseini, S.M., Akhlaghi, M., and Shakeri, M.: Transient heat conduction in functionally graded thick hollow cylinders by analytical method. Heat. Mass. Transfer. **43**, 669-675 (2007).
3. Shao, Z.S.Ma, G.W.: Thermo-mechanical stresses in functionally graded circular hollow cylinder with linearly increasing boundary temperature. Compos. Struct. **83**, 259-265 (2008).
4. Tarn, J.-Q.: Exact solutions for functionally graded anisotropic cylinders subjected to thermal and mechanical loads. Int.J.Solids Struct. **38**, 8189-8206 (2001).
5. Liew, K.M., Kitipornchai, S., Zhang, X.Z., et al.: Analysis of the thermal stress behaviour of functionally graded hollow circular cylinders. Int.J.Solids Struct. **40**, 2355-2380 (2003).
6. Valdevit, L., Hutchinson, J.W., and Evans, A.G.: Structurally optimized sandwich panels with prismatic cores. Int.J.Solids Struct. **41**, 5105-5124 (2004).
7. Valdevit, L., Wei, Z., Mercer, C., et al.: Structural performance of near-optimal sandwich panels with corrugated cores. Int.J.Solids Struct. **43**, 4888-4905 (2006).
8. Alavi Nia, A.Sadeghi, M.Z.: The effects of foam filling on compressive response of hexagonal cell aluminum honeycombs under axial loading-experimental study. Mater. Design. **31**, 1216-1230 (2010).
9. Seepersad, C.C., Dempsey, B., Allen, J.K., et al.: Design of multifunctional honeycomb materials. AIAA J. **42**, 1025-1033 (2004).
10. Guj, L.Sestieri, A.: Dynamic modeling of honeycomb sandwich panel. Arch Appl Mech. **77**, 779-793 (2007).
11. Nakamoto, H., Adachi, T., and Higuchi, M.: Approximate analysis of progressive deformation in honeycomb structures subjected to in-plane loading. Arch Appl Mech. **83**, 379-396 (2013).
12. Lu, T., Valdevit, L., and Evans, A.: Active cooling by metallic sandwich structures with periodic cores. Prog. Mater. Sci. **50**, 789-815 (2005).
13. Valdevit, L., Pantano, A., Stone, H., et al.: Optimal active cooling performance of metallic sandwich panels with prismatic cores. Int. J. Heat Mass Tran. **49**, 3819-3830 (2006).
14. Seepersad, C., CAllen, J., McDowell, D., et al.: Multifunctional topology-design of cellular material structures. J Mech Design. **130**, 1-13 (2008).
15. Valdevit, L., Vermaak, N., Zok, F., et al.: A Materials Selection Protocol for Lightweight Actively Cooled Panels. J. Appl. Mech. **75**, 061022 (2008).
16. Wang, B.Cheng, G.D.: Design of cellular structures for optimum efficiency of heat dissipation. Struct. Multidisc. Optim. **30**, 447-458 (2005).
17. Deng, J., Yan, J., and Cheng, G.: Multi-objective concurrent topology optimization of thermoelastic structures composed of homogeneous porous material. Struct. Multidisc. Optim. **47**, 583-597 (2013).
18. Liu, T., Deng, Z., and Lu, T.: Structural modeling of sandwich structures with lightweight cellular cores. Acta Mech. Sinica. **23**, 545-559 (2007).
19. Zhou, J., Deng, Z., Liu, T., et al.: Elastic structural response of prismatic metal sandwich tubes to

internal moving pressure loading. Int. J. Solids Struct. **46**, 2354-2371 (2009).
20. Zhou, J., Deng, Z., and Xu, D.: Dynamic response of prismatic metallic sandwich tubes under combined internal shock pressure and thermal load. Compos. Struct. **94**, 166-176 (2011).
21. Zhang, K., Deng, Z., Ouyang, H., et al.: Design and homogenization of me tal sandwich tubes with prismatic cores Struct. Eng. Mech. **45**, 435-450 (2013).
22. Lu, T.Chen, C.: Thermal transport and fire retardance properties of cellular aluminium alloys. Acta Mater. **47**, 1469-1485 (1999).
23. Gu, S., Lu, T., and Evans, A.: On the design of two-dimensional cellular metals for combined heat dissipation and structural load capacity. Int. J. Heat Mass Tran. **44**, 2163-2175 (2001).
24. Cheng, C., Fan, W., Cao, J., et al.: Heat Transfer across the Interface between Nanoscale Solids and Gas. ACS Nano. **5**, 10102-10107 (2011).
25. Ootao, Y.Tanigawa, Y.: Three-dimensional solution for transient thermal stresses of an orthotropic functionally graded rectangular plate. Compos. Struct. **80**, 10-20 (2007).
26. Tanigawa, Y., Oka, N., Akai, T., et al.: One-Dimensional Transient Thermal Stress Problem for Nonhomogeneous Hollow Circular Cylinder and Its Optimization of Material Composition for Thermal Stress Relaxation. JSME Int.J. A- Mech. Mater. Eng. **40**, 117-127 (1997).
27. Hohe, J.Librescu, L.: Advances in the Structural Modeling of Elastic Sandwich Panels. Mech. Adv. Mater. Struc. **11**, 395 - 424 (2004).